2008-01-2923

Advanced Diagnostics of Aircraft Electrical Generators

Freeman Rufus Jr., Seungkoo Lee and Ash Thakker
Global Technology Connection, Inc.

Sean A. Field and Nathan Kumbar
NAVAIR

ABSTRACT

The electrical and mechanical failures (such as bearing and winding failures) combine to cause premature failures of the generators, which become a flight safety issue forcing the crew to land as soon as practical. Currently, diagnostic / prognostic technologies are not implemented for aircraft generators where repairs are time consuming and its costs are high. This paper presents the development of several algorithms to differentiate between these failure modes and normal aircraft operational modes, determine the degree of damage and remaining life of a generator. P-3 generator data (vibrations & phase voltages/currents) were collected for a seeded bearing failure involving lubrication defects in main bearing system. The results show that the frequency domain analysis of the generator's phase voltage can be used to detect its general health and impending bearing failures.

INTRODUCTION

The P-3 Navy aircraft uses a Bendix (later AlliedSignal and currently Honeywell) generator that was designed over 30 years ago. The P-3 generator is a salient 8-pole (8 rotor bars), 6,000-rpm, 3-phase brushless ac generator. The running speed of the generator is 5700 rpm to 6,300 rpm (line frequency of 380 Hz to 420 Hz). The rated voltage and power is 115 VAC and 60 kVA (20 kVA/phase), respectively. It has a 12-pole ac exciter and a three-phase, half-wave diode rectifier rotating with the exciter armature and main generator field assembly. A single-phase permanent magnet generator (PMG) furnishes control voltage and power for the voltage regulator.

The electrical and mechanical issues (due to continuously operated beyond design point and less than optimal drive end bearing support) combine to cause premature failures of the P-3 generators, which become a flight safety issue forcing the crew to land as soon as practical. In case of a catastrophic failure, besides loosing a costly asset, components flying out of the generator sometime damage the airframe and surrounding equipment. Repairs are time consuming and its costs are high. Currently, diagnostic / prognostic technologies are not implemented for P-3 generators and other electrical power systems. Although some time series data (such as phase voltage and current) are collected during ground testing, no time series data is collected in-flight for the generators. Figure 1 shows the disassembled parts of a brushless ac generator for the P-3.

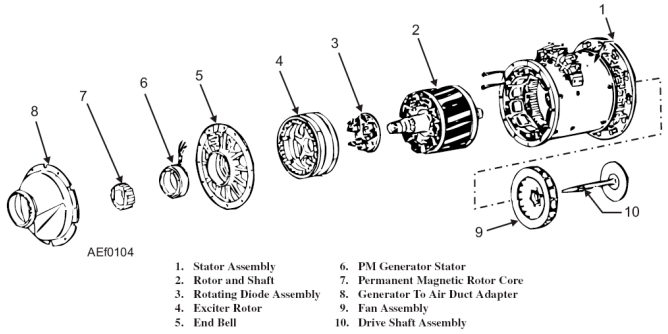

Figure 1: Disassembled brushless ac generator

A data-driven, diagnostic and prognostic architecture based upon fuzzy neural networks and Electrical Signature Analysis (ESA) approach is proposed in this work to detect and identify critical incipient generator failure modes and predict the remaining generator life under different operating conditions. This will enhance the reliability of aircraft generators by providing the crew and maintenance personnel with information about the current health state and remaining life of generators so that timely action can be taken.

MAIN SECTION

GENERATOR HEALTH MONITORING ALGORITHMS – Figure 2 depicts the basic modules of the proposed Diagnostic and health management system architecture based upon data-driven algorithms [1][2][3] and also shows how the architecture can provide inputs to the condition-based maintenance (CBM) module for maintenance execution. The feature extraction unit

takes raw sampled data from a generator and converts it to a form suitable for the diagnostic and prognostic modules. The diagnostician monitors continuously critical feature data and decides upon the existence of impending or incipient failure conditions. The detection and identification of an impending failure triggers the prognosticator. The prognosticator reports the remaining useful lifetime of the failing machine or component to the CBM module. The CBM module schedules the maintenance so that uptime is maximized while certain constraints are satisfied. The prognostic architecture is based on three constructs: 1) a static "virtual sensor" that relates known measurements to material deterioration; 2) a predictor which attempts to project the current state of the damaged material into the future thus revealing the time evolution of the damage and allowing the estimation of the material's remaining useful lifetime; and 3) a Confidence Prediction Neural Network (CPNN) [4][5] whose task is to account for uncertainty and manage/shrink the prediction bounds.

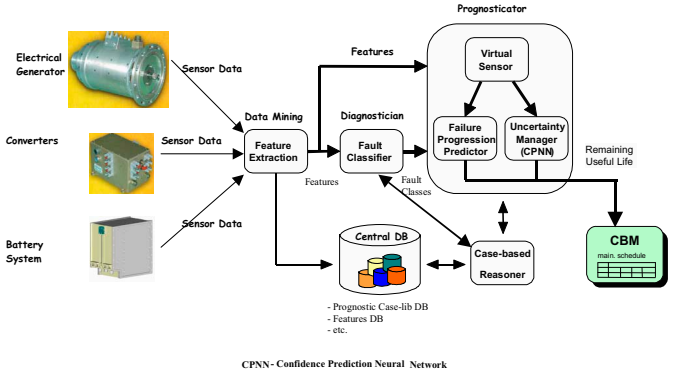

Figure 2: Overall Architecture for Diagnostic and Prognostic Assessment of Aircraft Electric Power Systems

Fuzzy Neural Networks – Recently, Fuzzy Neural Networks (FNNs) have been used for implementing fuzzy logic systems. FNNs combine the low-level learning and the computational power of neural networks with high-level reasoning and decision making of fuzzy systems [6]. The fuzzy neural structure proposed in [6] will be considered in this paper. This FNN structure consisted of a fuzzy rule base of Takagi-Sugeno fuzzy rules with the rule consequents being linear polynomials of the input premise variables. Both structure learning and parameter learning was used to adaptively develop the FNN construct. The structure learning was used to insert new membership functions, create new fuzzy rules and select initial parameters of the new rules on the basis of the desired output data. The parameter learning updated the consequent weights and the mean and standard deviation of the gaussian membership functions via the back propagation algorithm.

FNN STRUCTURE – The fuzzy neural architecture is divided into the premise part, the consequent part and the defuzzification part, as shown in Figure 3. The premise module partitions the premise space, assigns membership functions to each premise cell and develops the rule base of fuzzy rules. The consequent module consists of the rule consequents being linear polynomials of the input premise variables. Finally, the defuzzification module combines the firing strengths of the rules and the rule output functions to provide the final system output. Therefore, this FNN construct realizes the fuzzification, fuzzy reasoning, and defuzzification functionalities of a connectional fuzzy inference mechanism.

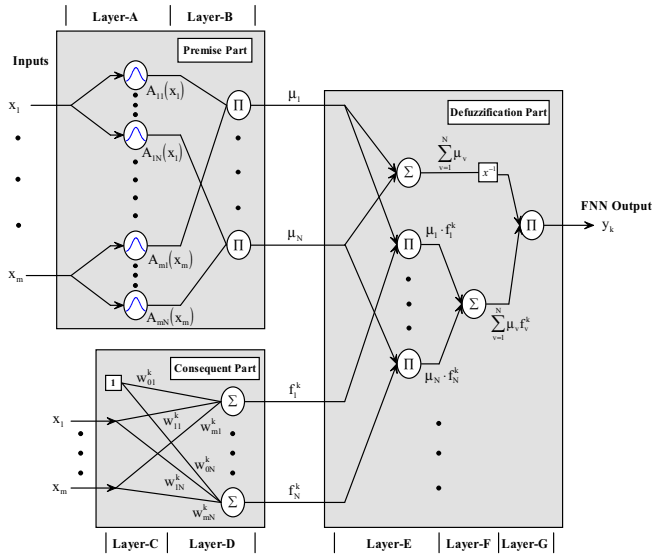

Figure 3: General configuration of the FNN architecture

OFFLINE / ONLINE LEARNING ALGORITHM – Structure learning inserts a new membership on each input axis that is not sufficiently covered by the existing memberships. New rules are created for the following cases: (1) the input is not covered by an existing rule and (2) if at least one new membership is created. A new fuzzy rule is created by combining the new memberships and an appropriate set of already existing memberships. Offline parameter learning updates the consequent weights via a local least squares estimation technique [7] using a set of training data. Online parameter learning updates the consequent weights via Kaczmarz's algorithm [7] applied to the current FNN input vector.

Feature Extraction – Initial time-domain and frequency domain feature extraction algorithms have been developed to distinguish between healthy and common failure modes such as bearing failure. The time domain features (kurtosis, root mean square, etc.) are calculated from (demodulated) voltage, current and/or vibration data. The frequency domain features are based upon ESA and power spectrum demodulation. The vector of features provided to the diagnostician and prognosticator will be composed of time domain statistics and statistical information about power spectral densities (PSDs) calculated at rotor, stator and bearing diagnostic frequencies.

POWER SPECTRUM DEMODULATION – In this work, the steps to perform power spectrum demodulation are (1) filtering of raw signal, (2) demodulation using Hilbert Transform based full wave rectification and (3) calculation of power spectrum via Welch method. The goal of this process is to remove the dominant line frequency component contained in the phase voltage and current signals so that ripple (composed of harmonics and fault signatures) along the line frequency can be analyzed using the envelope of the raw voltage/current signals. This approach allows a clear detection of failure frequencies without being swamped by the power in the line frequency. The Hilbert transform can be expressed as follow:

$$\hat{x}(t) = \frac{1}{\pi} \int_{-\infty}^{\infty} \frac{x(\tau)}{t-\tau} d\tau \quad (1)$$

The Hilbert transform creates an artificial complex signal $u(t) = x(t) + j\hat{x}(t)$ from input signal $x(t)$. The real part of the analytical signal is the original signal $x(t)$, the imaginary part $\hat{x}(t)$ represents the Hilbert transform of a real part, $x(t)$. The absolute value magnitude of the complex analytical signal forms the signal envelope and demodulates the original signal *x(t)*. The absolute value magnitude of u(t) is given by $|u(t)| = \sqrt{x^2(t) + \hat{x}^2(t)}$.

ELECTRICAL SIGNATURE OF GENERATOR FAILURES – ESA is the term used for the evaluation of the voltage and current waveforms. This provides an increased advantage to diagnostics as power-related, motor-related and load-related signals can be quickly compared. A key consideration when using ESA is that voltage signatures relate to the upstream of the circuit being tested (towards power generation) and current signatures relate to the downstream of the circuit being tested (towards the motor and load) as depicted in Figure 4. ESA uses the machine being tested as a transducer, allowing the user to evaluate the electrical and mechanical condition from the control or switchgear. For accurate analysis, ESA systems rely upon FFT analysis, much the same as vibration analysis.

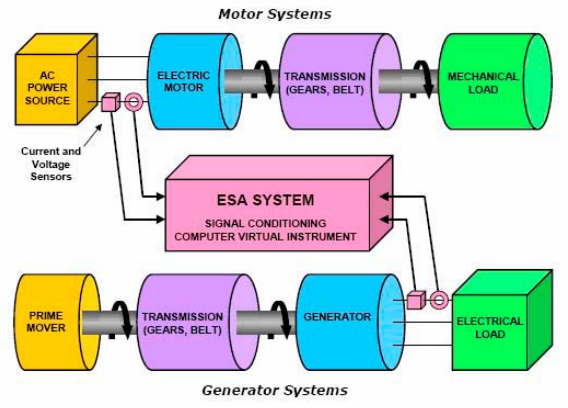

Figure 4: Applying ESA to Motor and Generator Systems

The following is a list of faults that can be detected using ESA and what is the corresponding characteristics/ patterns of the electrical signatures [8][9][10][11]:

- **Stator Mechanical Faults (loose coils, stator core movement, etc.):** CF = RS x Stator Slots; CF has line frequency sidebands.
- **Stator Shorts (shorted windings):** CF = RS x Stator Slots; CF has line frequency sidebands with running speed sidebands.
- **Rotor Indicator:** CF = RS x Rotor Bars; CF has line frequency sidebands.
- **Static Eccentricity:** CF = RS x Rotor Bars; CF has line frequency and twice line frequency sidebands.
- **Dynamic Eccentricity:** CF = RS x Rotor Bars; CF has line frequency and twice line frequency sidebands with running speed sidebands.
- **Mechanical Unbalance (and Misalignment):** CF = RS x Rotor Bars; CF has line frequency sidebands, space of four times line frequency then two line frequency peaks
- **Bearings:** CF_{BPOR} = BPOR x RS, CF_{BPIR} = BPIR x RS, CF_{2xBSF} = 2 x BSF x RS and CF_{FTF} = FTF x RS; CF_{BPOR}, CF_{BPIR} , CF_{2xBSF} and CF_{FTF} have line frequency sidebands. Harmonics of the frequencies can be found by multiplying each bearing frequency by integers with line frequency sidebands around each.

where **CF** is the center frequency of the fault pattern, **RS** is the running speed of the generator, line frequency (**LF**) is given as LF = [RS x NP]/2, **NP** is the number of poles, **BPOR** is the ball pass outer race, **BPIR** is the ball pass inner race, **2xBSF** is the 2 times the ball spin frequency and **FTF** denotes the fundamental train frequency. The bearing parameters needed to calculate BPOR, BPIR, 2xBSF and FTF are obtained from a manufacturer's catalog given the particular manufacturer and size of the bearing. Equation (2) depicts the frequency calculations for bearing failures where the parameters are as follows: B is the rolling element diameter, P is the pitch diameter, Φ is the contact angle and N is the number of rolling elements.

$$\begin{aligned} FTF &= \frac{1}{2}\left(1 - \frac{B}{P}\cos\Phi\right) \\ BPOR &= \frac{N}{2}\left(1 - \frac{B}{P}\cos\Phi\right) \\ BPIR &= \frac{N}{2}\left(1 + \frac{B}{P}\cos\Phi\right) \\ BSF &= \frac{P}{2B}\left(1 - \frac{B^2}{P^2}\cos^2\Phi\right) \end{aligned} \quad (2)$$

Fault Classifier – The diagnostician, implemented as a multiple-input multiple-output FNN, serves as a nonlinear discriminator to classify impending faults. The fault classifier is trained to recognize generator faults from a vector of features corresponding to rotor, stator and bearing failures.

Virtual Sensor – The virtual sensor calculates a failure measure indirectly through a neural network mapping of features and operating condition. It is often true that machine or component faults are not directly accessible for monitoring their growth behavioral patterns. Consider, for example, the case of an electrical generator. No direct measurement of the degree of stator / rotor winding degradation, bearings damage, etc. occurring in a generator is possible when it is in an operational state. That is, there is no such device as a "fault meter" capable of providing direct measurements of the fault evolution. A schematic representation of a virtual sensor for aircraft generator diagnostic is shown in Figure 5. The fault dimensions take the form of a vector of integer state-of-health (SOH) values where the values range from 100 (healthy) to 0 (fault)

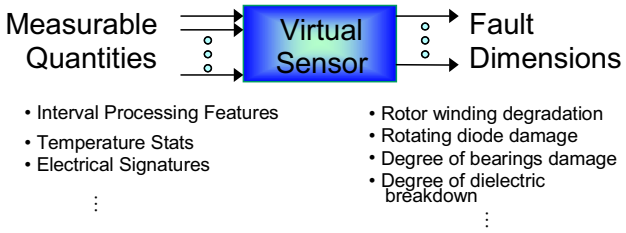

Figure 5: A schematic representation of the Virtual Sensor

Table 1: Failure modes common to wound field generators

Component	Failure Modes	Symptoms
Main Bearing	Wear	Increased vibration
Rotating Diodes	Short circuited diode(s)	• Increased current → generator running hot • Eventual insulation failure • Loss of regulation → generator tripping offline
Main Rotor Field	Inter-turn short circuited field	• Increased vibration • Increased field current
Main Stator	Short circuit winding(s): -- turn-to-turn	• Intense heat • Insulation damage • Excessive current flow
Airgap Zone	Static and dynamic eccentricity	• Increased vibration • Insulation degradation • Rotor / stator rubbing
Loss of Cooling (Fan or Pump)	Blockages Wear	Increased stator temperatures

FAILURE MODES COMMON TO WOUND FIELD GENERATORS – In this section, we define typical failure modes for the P-3 generator that are universal to all wound field generators regardless of the cooling mechanism (Air, Conduction and Oil Spray cooling). Presently, when main stator and rotor opened field failures occur, they will cause the generator to immediately drop offline as protection to the system or simply because the generator can not work under the failure condition. Other failure modes that have poor diagnostic potential are open circuit rotating diodes and phase-to-phase short circuit stator windings.

Table 1 lists common generator failure conditions that are generic to wound field generators and can be diagnosed prior to loosing the generator because these failures allow the generator to continue operation in a degraded condition. These failures are more easily diagnosed and can initiate preventive maintenance prior to failure. Additionally, reduction in cooling efficiency can also be detected utilizing resistive temperature devices.

GENERATOR DRIVE-END BEARING FAILURE EXAMPLE – A small amount of Silicon Carbide grit was added to the lubrication for the "drive end" bearing of a P-3c generator to accelerate degradation of the bearing system while data was collected for a span of ~3,320 seconds until the main bearing died. Triaxial acceleration vibrations, electrical stator phase currents and voltages were collected at 100 kHz for the seeded main bearing failure. Also, the signal from the bearing failure indication system, which failed to indicate bearing failure, was recorded throughout the testing. The *running speed* and load of the generator was 100 Hz and 60 kVA, respectively. The vibration data did not indicate bearing failure via visual inspection alone. In particular, no large spikes in vibration data were observed and no significant change in the power spectral density of original vibration signals were seen during the experiment.

Comparison of Low-hour and Degraded Generators – The generator with seeded bearing fault was contrasted with NAVAIR provided data collected at 100 kHz for 3 low-hour P-3 generators (Gen 73-A0255, Gen 1182 and Gen 18700071). The rotor indicator ($CF_{RS \times Rotor\ Bars}$) and key bearing diagnostic frequencies (CF_{FTF}, CF_{BPOR}, CF_{BPIR} and CF_{2xBSF}) were determined to be 800 Hz, 39.95 Hz, 359.58 Hz, 540.42 Hz and 463.18 Hz, respectively. These values were calculated using Equation (2) and the following parameters: B is 0.375 inches, P is 1.81 inches, N is 9, Φ is 14.1° (0.246 radians), number of rotor bars is 8 and the running speed is 100 Hz.

Figures 6 through 8 show the normalized power spectrum of the demodulated voltage signal as a function of time and harmonics of key frequencies for 3 low-hour

generators and a generator with seeded bearing failure. The normalized power spectrum was calculated as PSD values minus the average PSD where any value below the threshold has a normalized power spectral density of zero. The key frequencies shown are harmonics of rotor indicator ($CF_{RS\ x\ Rotor\ Bars}$) and two bearing diagnostic frequencies (CF_{FTF} and CF_{BPOR}). Two of the low-hour generator depicted in Figure 8 consistent behavior until about 24 kHz while 'Gen 1182' showed significant change around 11.4 kHz. Unlike the low-hour generators, the generator with seeded bearing fault has large drops in PSDs in the range of 3.2 kHz and 50 kHz from expected values. Likewise, Figures 7 and 8 show that bearing frequencies showed more consistency in PSD values for low-hour generators than the generator with seeded fault.

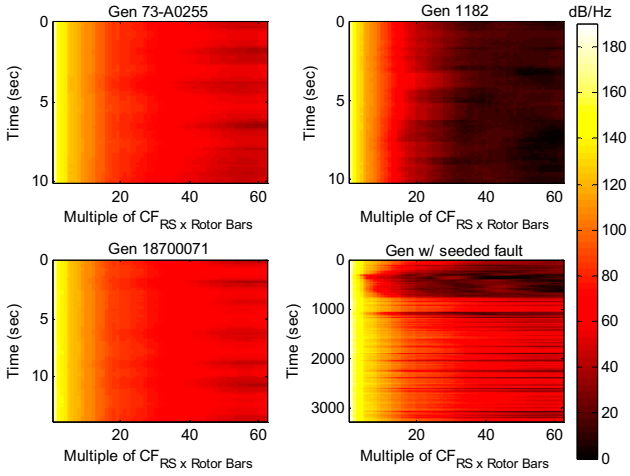

Figure 6: Normalized power spectrum of generators for harmonic frequencies of $CF_{RS\ x\ Rotor\ Bars}$ (800 Hz)

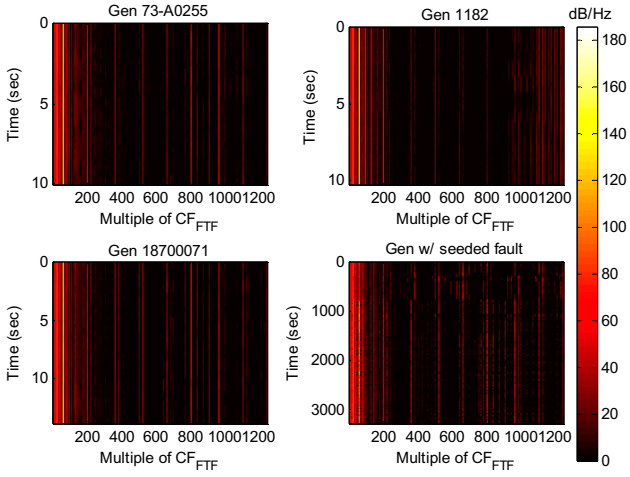

Figure 7: Normalized power spectrum of generators for harmonic frequencies of CF_{FTF} (39.95 Hz)

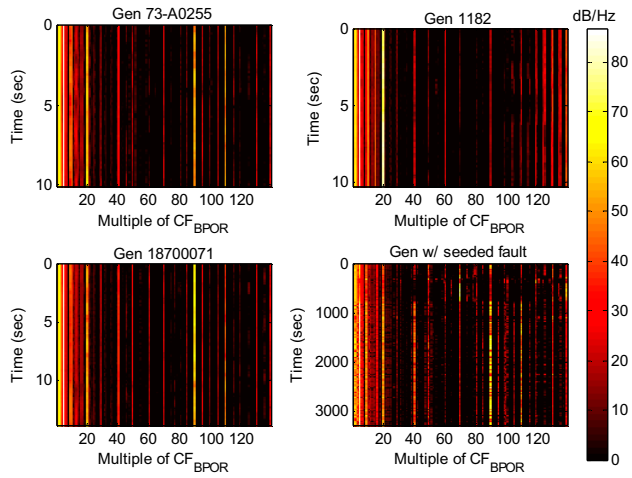

Figure 8: Normalized power spectrum of generators for harmonic frequencies of CF_{BPOR} (359.58 Hz)

Diagnostic Features – Figure 9 shows 1D view of the range in PSDs values for rotor indicator diagnostic frequencies for the 4 generators. It is clearly seen that the low-hour generators have less range than the generator with seeded fault. Also, the range in PSDs for each multiple of $CF_{RS\ x\ Rotor\ Bars}$ increases as a function of harmonic order. This behavior is similarly observed for harmonics of the four key bearing frequencies. Figure 10 shows the range in PSDs for harmonics of CF_{BPOR}. Therefore, the following three general features were selected to detect bearing failures:

- $PSD_{max\ diff}$ = [PSD_{max} – PSD_{min}] per diagnostic frequency
- $PSD_{std\ dev}$ per diagnostic frequency
- PSD_{max} (or Peak PSD) per diagnostic frequency.

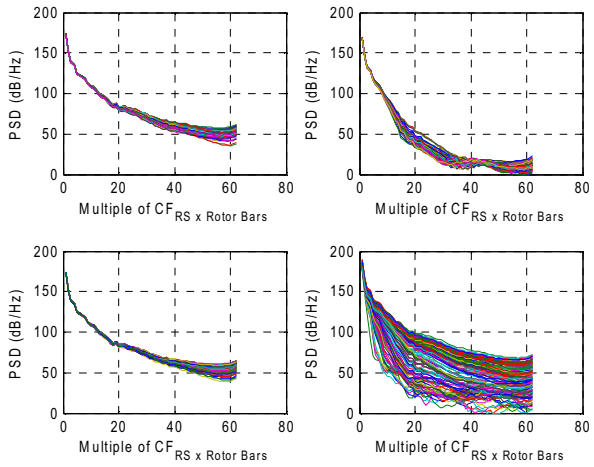

Figure 9: Range of PSD values for rotor indicator diagnostic frequencies

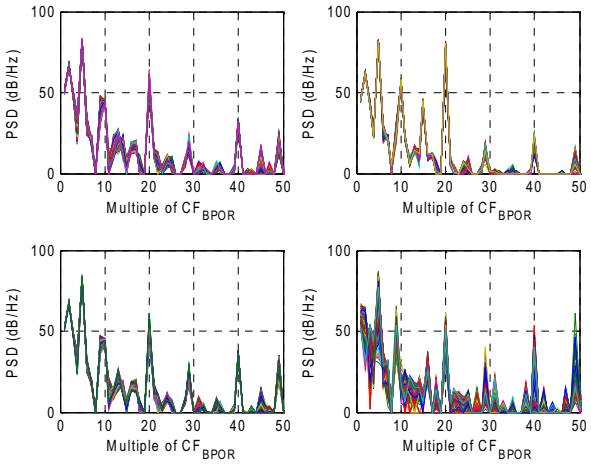

Figure 10: Range of PSD values for CF_{BPOR} diagnostic frequencies

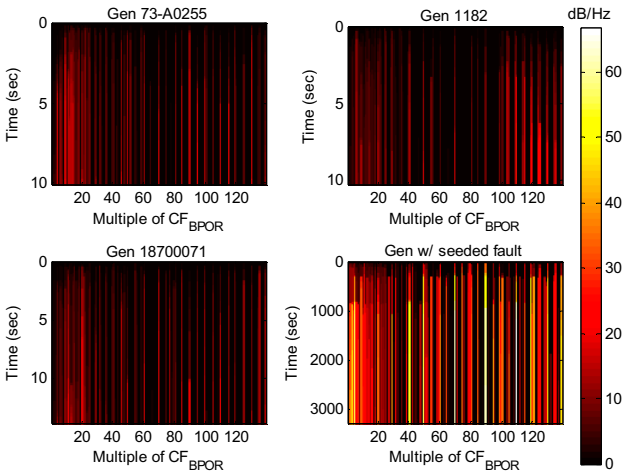

Figure 12: $PSD_{max\ diff}$ as a function of time and harmonics of CF_{BPOR}

Results – Figures 11 and 12 show that the $PSD_{max\ diff}$ per rotor and BPOR diagnostic frequencies is an excellent feature in distinguishing between low-hour and degraded generators. Both figures show significant changes in values of $PSD_{max\ diff}$ for the seeded fault generator at 300 seconds and 780 seconds into experiment which are well before the bearing system died. This feature was also able to detect that the rotor health was different from low-hour generators as early as 20 seconds into the experiment.

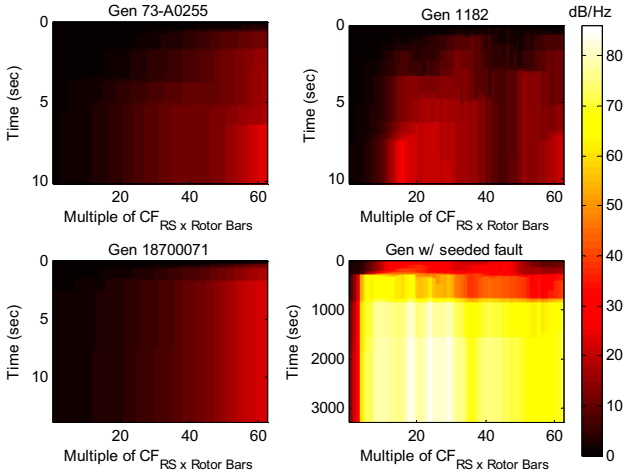

Figure 11: $PSD_{max\ diff}$ as a function of time and harmonics of $CF_{RS\ x\ Rotor\ Bars}$

Figures 13 and 14 show how the accumulation of $PSD_{max\ diff}$ w.r.t. frequency evolves over time for the rotor and bearing diagnostic frequency during the seeded bearing fault experiment. The accumulated $PSD_{max\ diff}$ metric for rotor diagnostic frequencies was above the threshold established from low-hour generators at 20 seconds and showed two significant changes in health of the generator: (1) 240 → 340 seconds and (2) 760 → 860 seconds. Note that the accumulated $PSD_{max\ diff}$ metric had little no change after 1820 seconds into the experiment. In the case of bearing diagnostic frequencies, the seeded fault generator exceeded the thresholds at 300 seconds into the experiment and exhibited a logarithm-like growth after 780 seconds until the end of the experiment. Therefore, the accumulated $PSD_{max\ diff}$ metric can be used an indicator of the generator's health and the degree of damage when encountering bearing failures.

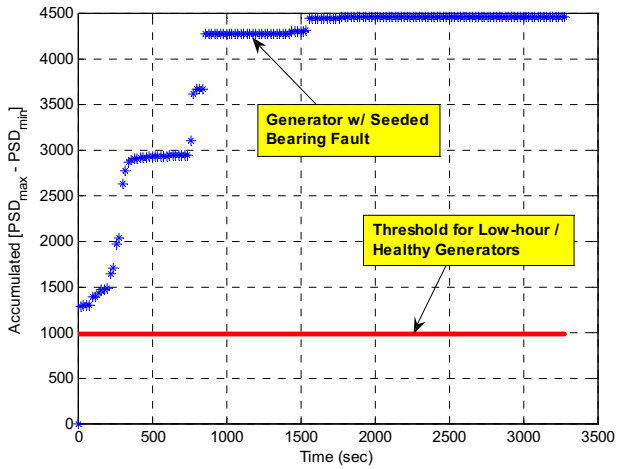

Figure 13: Accumulated $PSD_{max\ diff}$ for harmonics of rotor diagnostic frequency

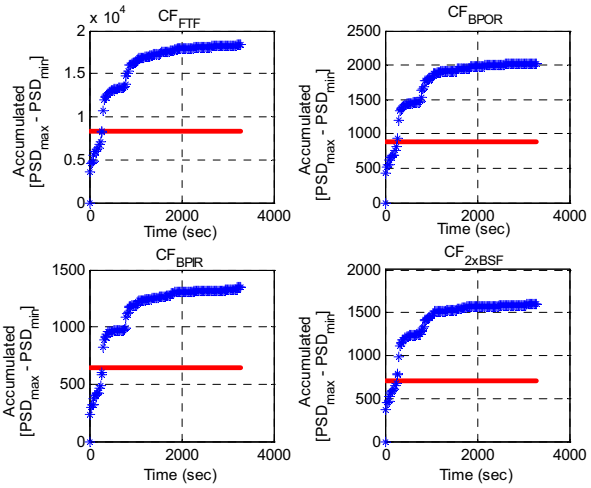

Figure 14: Accumulated $PSD_{max\ diff}$ for harmonics of bearing diagnostic frequencies

CONCLUSION

Common generator failure conditions that are generic to wound-field generators such as the P-3 generator were determined along with corresponding electrical signatures. Frequency domain features were developed to distinguish between healthy and degraded generators experiencing impending bearing failures using demodulated phase voltage. The results show that the accumulation of the max difference in PSD values per rotor and bearing diagnostic frequencies can be used to detect an aircraft generator's general health and impending bearing failures well before failure occurs. The accumulated $PSD_{max\ diff}$ metric for rotor and bearing diagnostic frequencies were able to detect as early as 20 seconds and 300 seconds into the seeded bearing fault experiment that the generator was operating in degraded state, respectively.

ACKNOWLEDGMENTS

The authors would like to thank Sean Field and Nathan Kumbar for the sponsorship of this research under NAVAIR contract number N68335-08-C-0131. In addition, the authors would like to thank Daryl Cox of Oak Ridge National Laboratory for collecting seeded bearing fault data, Scott Jacobs of Innovative Power Solutions for providing a list of common wound field generator failures, and NAVAIR for providing electrical / vibration test data for several low-hour P-3 generators.

REFERENCES

1. Zhang, G., Lee, S., Propes, N., Zhao, Y., Vachtsevanos, G., Thakker, A., and Galie, T., "A Novel Architecture for an Integrated Fault Diagnostic/Prognostic System," *AAAI Symposium*, Stanford, California, March 25-27, 2002.
2. Wang, P. and Vachtsevanos, G., "Fault Prognosis Using Dynamic Wavelet Neural Networks," *AAAI Spring Symposium*, Polo Alto, March 22-24, 1999.
3. Vachtsevanos, G. and Wang, P., "A Wavelet Network Framework for Diagnostics of Complex Engineered Systems," *Proceedings of MARCON 98 Maintenance and Reliability Conference*, Knoxville, TN, May 12-14, 1998, (invited paper).
4. Tsui, F.C., Sun, M.G., Li, C.C., Sclabassi, R.J., "A wavelet based neural network for prediction of ICP signal" *Proceedings of 1995 IEEE Engineering in Medicine and Biology 17th Annual Conference and 21 Canadian Medical and Biological Engineering*, p.1045-6, vol.2, 20-23 Sept. 1995.
5. He, S.C. and He, Z.Y., "Blind equalization of nonlinear communication channels using recurrent wavelet neural networks", *1997 IEEE International Conference on Acoustics, Speech, and Signal Processing*, p.3305-8, vol.4, 21-24 April 1997.
6. Rao, S.S. and Kumthekar, B., "Recurrent wavelet networks", Proceedings of the 1994 *IEEE International Conference on Neural Networks*, p 3143-3147, Orlando, FL, USA, 1994.
7. Rufus, F., Vachtsevanos, G. and Heck, B., "Adaptive Mode Transition Control of Nonlinear Systems Using Fuzzy Neural Networks," *8th IEEE Mediterranean Conference on Control & Automation*, University of Patras, Rio, Greece, July 17-19, 2000.
8. Penrose, H. W., "Electrical Motor Diagnostics for Generators Part 1: The Basics," ALL-TEST Pro, 2005, http://www.reliabilityweb.com/art06/generator_diagnostics.htm
9. Penrose, H. W., "Practical Motor Current Signature Analysis Taking the Mystery Out of MCSA," ALL-TEST Pro, 2005, www.alltestpro.com/pdf/PracticalSignatureAnalysis.pdf
10. Nandi, S., Toliyat, H. A., and Li, X., "Condition Monitoring and Fault Diagnosis of Electrical Motors—A Review," *IEEE Transactions On Energy Conversion*, VOL. 20, NO. 4, December 2005, pp. 719 – 729.
11. Liu, L., "Robust Fault Detection and Diagnosis for Permanent Magnet Synchronous Motors," Phd Thesis, Florida State University, Summer 2006.

CONTACT

F. Rufus, Jr. is with Global Technology Connection, Inc., Atlanta, GA 30339 USA (phone: 770-803-3001 x29; fax: 770-234 4148; e-mail: frufus@globaltechinc.com; web address: www.globaltechinc.com).